

Earth and Space Science



RESEARCH ARTICLE

10.1029/2020EA001572

Key Points:

- Comparison between sea-bottom and satellite altimeter-derived gravity allowed to estimate the noise effects in altimeter data, near-shore
- The high-resolution sea-bottom gravity available along the Italian coasts detects effects of sources not seen by satellite altimeter data
- Combined analysis of satellite altimeter and sea-bottom gravity gives a complete view on the offshore continuation of near-shore structures

Correspondence to:

L. S. Zampa,
lzampa@inoogs.it

Citation:

Zampa, L. S., Lodolo, E., Creati, N., Busetti, M., Madrussani, G., Forlin, E., & Camerlenghi, A. (2022). A comparison between sea-bottom gravity and satellite altimeter-derived gravity in coastal environments: A case study of the Gulf of Manfredonia (SW Adriatic Sea). *Earth and Space Science*, 9, e2020EA001572. <https://doi.org/10.1029/2020EA001572>

Received 18 NOV 2020

Accepted 16 MAR 2022

Author Contributions:

Conceptualization: L. S. Zampa
Data curation: G. Madrussani, E. Forlin
Formal analysis: L. S. Zampa, E. Lodolo, N. Creati, G. Madrussani
Methodology: L. S. Zampa, E. Lodolo, N. Creati, G. Madrussani
Resources: E. Forlin, A. Camerlenghi
Software: L. S. Zampa, N. Creati, G. Madrussani
Supervision: E. Lodolo, N. Creati, M. Busetti, A. Camerlenghi
Validation: E. Lodolo, N. Creati, M. Busetti, G. Madrussani
Writing – original draft: L. S. Zampa, E. Lodolo

© 2022 The Authors.

This is an open access article under the terms of the Creative Commons Attribution-NonCommercial License, which permits use, distribution and reproduction in any medium, provided the original work is properly cited and is not used for commercial purposes.

A Comparison Between Sea-Bottom Gravity and Satellite Altimeter-Derived Gravity in Coastal Environments: A Case Study of the Gulf of Manfredonia (SW Adriatic Sea)

L. S. Zampa^{1,2} , E. Lodolo¹, N. Creati¹ , M. Busetti¹ , G. Madrussani¹, E. Forlin¹, and A. Camerlenghi¹ 

¹National Institute of Oceanography and Applied Geophysics—OGS, Sgonico, Italy, ²Department of Mathematics and Geosciences, University of Trieste, Trieste, Italy

Abstract The marine gravity field derived from satellite altimetry is generally biased in coastal areas by signals back-scattered from the adjacent land. As a result, the derived gravity anomalies are generally unreliable for geophysical and geological interpretations of near-shore environments. We compared two different altimetry models with sea-bottom gravity measurements acquired along the Italian coast to quantify the errors generated by reflections from onshore areas and verify the quality of the geologic models inferred from gravity data. We focused on the Gulf of Manfredonia, in the SE sector of the Adriatic Sea, where (a) two different sea-bottom gravity surveys have been conducted over the years, (b) the bathymetry is mainly flat, and (c) seismic data has revealed a prominent carbonate ridge covered by hundreds of meters of Oligocene-Quaternary sediments. Gravity field derivatives have been used to enhance both deep geological contacts and coastal noise. The analyses point to a ringing noise that degrades the altimeter signals up to 17 km from the coast. Differences between observations and gravity calculated from a geological model and constrained by seismic data show that all the data sets investigated register approximately the same interference patterns associated with the Gondola Fault Zone. This study shows the potential for integrating gravity anomalies from satellite altimetry with high-resolution near-shore data, such as that provided by sea-bottom gravity network available around the Italian coasts. Future applications will use this technique to improve the analysis of the connections between marine and inland geology in transitional areas.

Plain Language Summary We present a comparative analysis between two types of gravity data used in geophysical studies: satellite altimeter-derived gravity and sea-bottom gravity. It is generally accepted that the quality of satellite altimetry data in the vicinity of the coast is impaired by signals reflected from nearby land. We show how this may affect the interpretation of gravity anomalies and how it could be solved by integrating altimetry-derived gravity data with high-resolution marine gravity networks in the proximity of coasts. We chose as a test area the Gulf of Manfredonia on the South Adriatic coast of Italy, which hosts a major tectonic feature, namely, the Gondola Fault Zone. The fault zone is not clearly expressed at the seafloor, which is generally flat, but it dislocates carbonate rocks located hundreds of meters below the sediments. In so doing, it creates lateral density contrasts that are detectable in the gravity data.

1. Introduction

The quality of sea-surface height measurements from satellite radar altimetry in coastal regions is impaired by the noisier radar returns from the generally rougher coastal sea and simultaneous returns from reflective land and inland water (Andersen & Knudsen, 2000). Satellite altimeter-derived gravity data in the vicinity of land is therefore inevitably contaminated by non-gravity signals.

The altimeter-derived results can be improved using the waveform tracking technique, which reprocesses waveform data through a “coastal retracking system,” as performed along the Australian coastal regions (Deng & Featherstone, 2006). The resolution of these methods has continuously improved in recent years, thanks in part to newly available and more accurate radar data. Moreover, radar altimetry has the advantage of near-global coverage and almost homogeneous error characteristics in non-coastal regions (Fu & Cazenave, 2000; Green et al., 2019). When comparative data acquired independently and with different techniques are available, such as marine geophysical measurements, it is possible to provide a more exhaustive and quantitative assessment of the satellite altimetry errors. From the early 1950s to the late 1980s, the Osservatorio Geofisico Sperimentale

Writing – review & editing: L. S. Zampa, E. Lodolo, N. Creati, M. Busetti, G. Madrussani, E. Forlin, A. Camerlenghi

(OGS) of Trieste (Italy) performed several gravimetric surveys along the Italian coasts using sea-bottom gravimeters (Ciani et al., 1960; Gantar, 1983; C. Morelli, 1966), during which thousands of data points were recorded (Figure 1).

In this study, we investigate the compatibility of sea-bottom gravity with satellite altimeter-derived gravity, using both the DTU13 (Andersen et al., 2014) and the S&S (Sandwell et al., 2014) data sets, and provide a quantitative evaluation of the differences between the two types of gravity data. To delineate the effectiveness of this comparison (satellite-derived gravity vs. sea-bottom gravity), this study focuses on a relatively small coastal area in the SW Adriatic Sea, the Gulf of Manfredonia, where two different sets of sea-bottom gravity data have been acquired over the years.

The choice of study area is essentially motivated by the following: (a) it is a very flat sector of the coastal region, where a thick, ellipsoidal-shaped sedimentary basin has been identified with seismic reflection profiles; (b) a dense grid of gravity measurements acquired at the sea-bottom is available; (c) seismic profiles show the presence of significant geological discontinuities propagating from inland (Gargano Peninsula) toward the offshore (Gulf of Manfredonia), and thus tend to be detectable within the gravity data; (d) it represents an ideal case in which the flat seafloor does not mimic the trend of the rock-basement below the seafloor sediments, which instead can be easily imaged using gravity anomalies.

The sea-bottom gravity stations in the study area were connected to the national absolute gravity network, which has been upgraded over the years leading to a systematic bias between data points taken in different periods. All measurements were concentrated near the coasts due to the vessel position being easier to triangulate from the land. In addition, the proximity of docking harbors guaranteed a fast and frequent connection with land-based gravity stations, thereby reducing large residual drift errors in the final absolute gravity values.

These data had never been coupled with sea-surface gravity, acquisition of which started in the 1960s (C. Morelli, 1966). The great advantage in terms of acquisition time and cost of sea-surface gravity over sea-bottom gravity has made this new datatype preferable and more widely used. However, sea-bottom measurements are still more sensitive to sub-bottom density variations and not affected by leveling errors in the same way as sea-surface gravity, which makes them more suitable when it comes to studying the accuracy of gravity fields near the coast (Ballu et al., 1998; Fairhead, 2016; Talwani et al., 1966).

All the gravity data sets analyzed in the current work have undergone preliminary correction using the same reference model: the Bouguer anomaly of sea-bottom data that takes into account the free-water gradient and gravity effects of topography and water masses above and below the sea-bottom station. Meanwhile, the same anomaly computed for the altimeter-derived data considers only the effects of topography and water masses above and below the sea surface, respectively.

We used the Integrated Second Vertical Derivative (ISVD) and the Tilt derivative to enhance both the noise effects and the gravity signals from the edges of causative sources. The results of these analyses were compared with those calculated from a forward gravity model derived from seismic-reflection data. This allowed us to investigate the relative sensitivity of each data set to the gravity effect of known sources and provided a better understanding of which data set would be easier to repair for the interpretation of gravity anomalies.

The results of this current work can be used in the study of continuity and configuration of geological contacts marked by density contrasts from inland to offshore coastal areas. The method described here could potentially be implemented to significantly reduce errors caused by coastal noise in satellite altimeter-derived gravity data in similar coastal regions where sea-bottom gravity measurements are available.

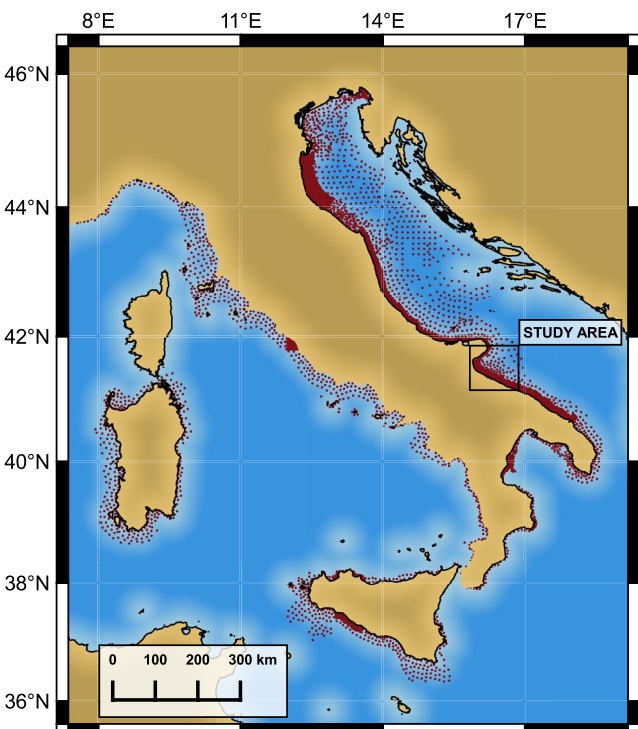


Figure 1. Position of sea-bottom gravity stations (small red dots) from the OGS database, including Gantar (1983). Most of the stations recorded from the early 1950s to the late 1980s, a few tens of kilometers from the Italian coasts, with an average spacing of about 1 km. Map frame in WGS 84/World Mercator + EGM2008 height coordinate system (EPSG: 6893).

1.1. Geological Setting

The Gulf of Manfredonia is located in the SW sector of the Adriatic Sea. It is bounded to the north by the Gargano Peninsula and to the west by the northern part of the Puglia region (i.e., the northern sector of the Salento). Within the gulf, the bathymetry shows maximum water depths of ~90 m, with a smooth seafloor surface that lacks any significant morphological features.

The lithostratigraphy of the area to a depth of ~2.5 km has been divided into four main units (D. Morelli, 2002; Volpi et al., 2015): (a) Plio-Quaternary sandy and clayey sediments, (b) upper Oligocene–Miocene argillaceous and marly turbidites, (c) middle Liassic-Paleogene pelagic limestones and marls, and (d) upper Triassic-lower Liassic evaporitic, dolomitic and shallow-water limestone. The two lowest units (iii) and (iv), which are generally called the “Jurassic-Paleogene carbonate succession,” form the solid bedrock. The bedrock is covered by unconsolidated or partially consolidated siliciclastic sediments up to depths of ~1,500 m in the deepest basin (Figure 2b).

Seismic studies conducted since 1970s have revealed the presence of an important structural element beneath the sedimentary cover, striking broadly W-E, known as the Gondola Fault Zone. The Gondola Fault Zone includes several E-W and NW-SE trending fault segments that define an elongated, buried structural high called the “Gondola ridge” (Colantoni et al., 1990; de Alteiris, 1995; de Alteiris & Aiello, 1993), which extends ~70 km across the shelf without producing significant morphologies at the seafloor along most of its extension (Ridente & Trincardi, 2006). Conversely, a tectonically related relief visibly affects the seafloor morphology downslope along the ~50 km-long NW-SE branches of the Gondola Fault Zone (de Alteiris, 1995; Tramontana et al., 1995). The Gondola Fault zone has been related to a Cenozoic reactivation of pre-existing faults (Finetti, 1983; Tramontana et al., 1995). Quaternary activity is evidenced by the deformation of Middle Pleistocene sediment. The overall geometry of the Gondola Fault Zone suggests a significant right-lateral component of motion (Ridente et al., 2008).

The Gondola fault system continues onshore with the Mattinata Fault that cuts through the Gargano Promontory (Figure 2a), which is an E-W elongated relief (maximum elevation ~1,000 m) along with the flexural bulge of the Adriatic foreland (Ridente et al., 2008). The Gondola and Mattinata fault zones can be traced for a total length of at least 180 km (Di Bucci et al., 2006), and belong to the ~15 km wide corridor of the fault system that extends from the Adriatic Sea to the core of the Apennines (Ridente et al., 2008). The Mattinata Fault is considered to be a poly-phased belt, subjected to an intense deformation since Mesozoic times and formed by multiple splay faults (see Billi et al. [2007], and references therein). However, seismic data have shown that the Mattinata Fault is neither in direct continuity nor perfectly aligned with the Gondola Fault Zone, showing an under-lap of ~20 km and right-stepping of ~5 km (Ridente et al., 2008).

2. Data

In this study, we calculate and compare gravity anomalies covering the Gulf of Manfredonia using four different data sets: two satellite altimeter-derived gravity data sets, that is, the DTU13 (Andersen et al., 2013, 2014, 2015) and the S&S (Sandwell et al., 2014), and two sea-bottom gravity data sets, that is, OGS60 (Ciani et al., 1960) and OGS83 (Gantar, 1983). To constrain the forward gravity model, we used the geological model produced by Volpi et al. (2015). The model is based on the interpretation of multichannel seismic profiles made available through the Visibility of Petroleum Exploration Data in Italy project (ViDEPI, www.videpi.com, managed by the Italian Ministry of Economic Development) and released in SEG-Y format by the web portal Seismic data Network Access Point (SNAP), managed by the Istituto Nazionale di Oceanografia e di Geofisica Sperimentale (Diviacco, 2018).

2.1. Satellite Altimeter Derived Gravity

Satellite altimeter gravity is derived from the Sea Surface Heights (SSH) measurements, obtained by radar satellites orbiting at 800 km and 1,300 km above the Earth’s surface. A microwave pulse emitted by the satellite antenna is reflected by a portion of the sea surface (the footprint), whose position is mapped relative to the reference ellipsoid. This allows for a complete reconstruction of the SSH over almost the entire globe. After

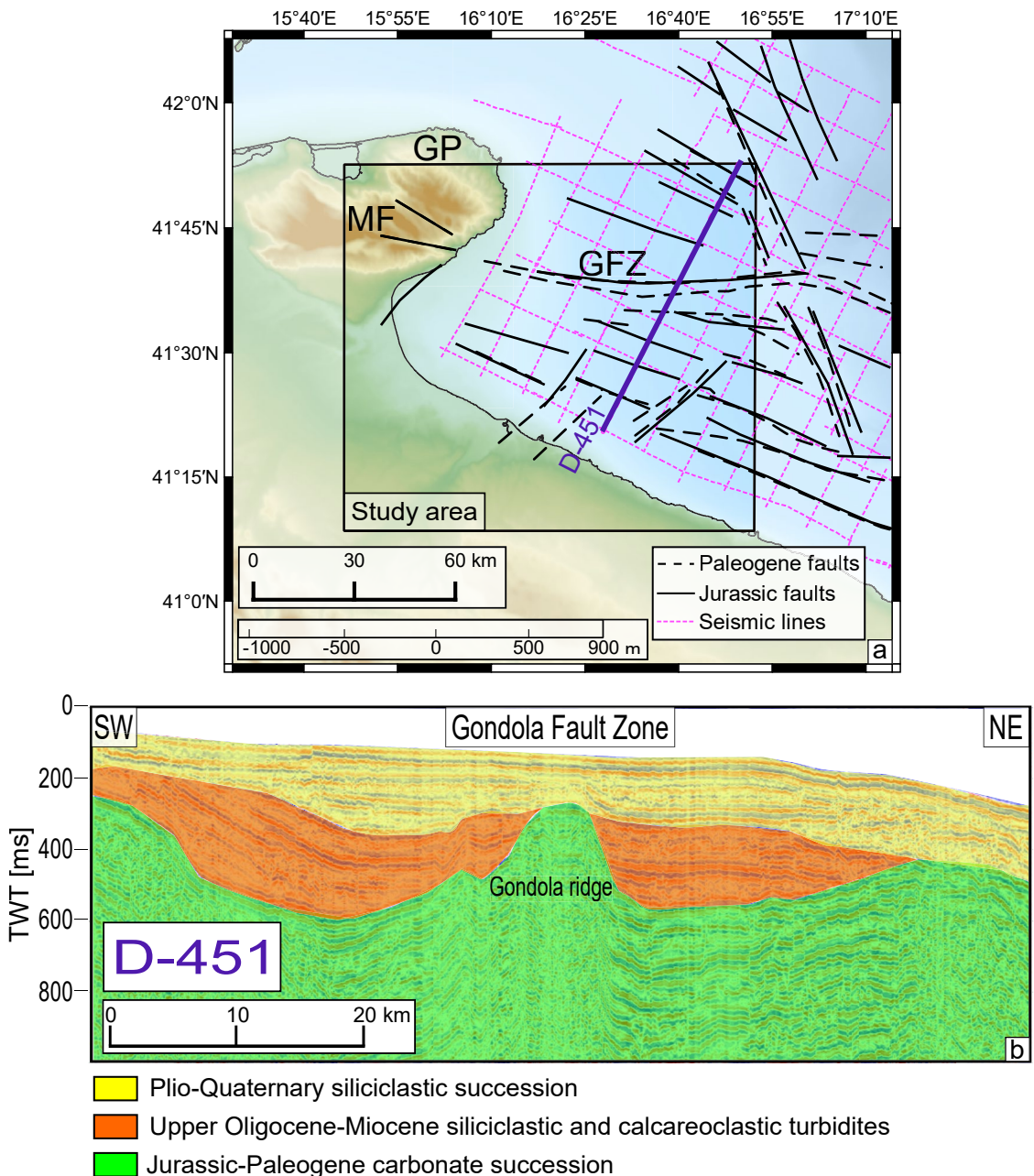


Figure 2. (a) Structural map of the Gulf of Manfredonia, showing the Gondola Fault Zone (GFZ) and its inland continuation with the Mattinata Fault (MF) cutting through the Gargano Promontory (GP). Fault interpretation in the marine sector has been derived from seismic data (D. Morelli, 2002), and position of the multichannel seismic profiles from ViDEPI (violet lines). (b) Seismic profile D-451 (position in Figure 2a), where the Gondola ridge is clearly imaged (interpretation of seismic layers has been taken from Volpi et al. (2015)). Seismic data comes from the project ViDEPI “Visibility of Petroleum Exploration Data in Italy” (URL: www.videpi.com), managed by the Ministry of Economic Development. Data have been made available in the SEG-Y format on the SNAP “Seismic data Network Access Point” platform, managed by the Istituto Nazionale di Oceanografia e di Geofisica Sperimentale, OGS (Diviacco, 2018).

correcting the SSH for time-dependent components, residual orbital errors, and the Mean Dynamic Topography (a quasi-stationary component of SSH), the result is a static realization of the marine geoid (Andersen et al., 2010). The mathematical relation between geoid undulations (N) and the Free-air anomaly (Fa) is given by the Bruns formula:

$$Fa = -g_{th}^s \frac{\partial N}{\partial r} - \frac{2}{R} N g_{th}^s \quad (1)$$

where g_{th}^s is the theoretical gravity (spherical approximation), r is the radius vector connecting the computational point to the center of the Earth, N is the geoid undulation, and R is the mean Earth radius.

There are two methods available to compute the vertical geoid gradient $\frac{\partial N}{\partial r}$, using altimetry data: (a) the "geoid-to-gravity" and (b) the "slope-to-gravity" method (Fairhead, 2016).

2.1.1. DTU13 Model

The DTU13 data set was obtained using the geoid-to-gravity method, developed by the Technical University of Denmark (Andersen et al., 2014). In this approach, the vertical derivative is computed starting from 2-D regular grids of the geoid. The geoid grids result from spatial interpolation of radar data, crossover adjusted, and corrected for time-variable and stationary components of the SSH, that is, all those components not directly related to the gravity field of the solid Earth (Andersen et al., 2010).

The derivative is calculated using the Fast Fourier Transform (FFT) after having removed the effect of the EGM2008 spherical harmonic model up to degree and order 2160 (Pavlis et al., 2012), that is, wavelengths of ≤ 20 km (Barthelmes, 2009). The removed harmonic components are then added back into the final result (remove-restore technique).

The resulting free-air anomaly is available in a grid format, with a sampling interval of 1 arc-minute. However, the real maximum resolution is limited by the along-track spacing of observations, which is around 7 km, and by the systematic use of a Wiener low pass filter with cut-off wavelengths ranging between 5 and 16 km (Andersen & Knudsen, 1998; Andersen et al., 2010). As a result, the shortest reliable wavelength is around full waveforms of ~ 13 km (Andersen, 2013; Fairhead, 2016).

The DTU13 model is associated with an interpolation error file (Figure 3b), showing uncertainties on the Mean Sea Surface grids (MSS_{err}), which is defined in units of meters (Andersen & Knudsen, 2009). This error file shows the quality of gridded data points, and it can be used to roughly identify the transition between land and ocean (Andersen et al., 2008). However, it may underestimate the real uncertainties of the MSS since it only accounts for interpolation errors and not for actual orbit errors, or other errors in various range corrections (Andersen & Knudsen, 2009).

The relationship between geoid and gravity (Equation 1) gives a ~ 1 mGal amplitude for a sea surface slope of 7 mm/7 km (Sandwell et al., 2013), that is, 1.4 mGal/cm when considering horizontal distances of 7 km (i.e., full-waveforms of 14 km). This simple equivalence has been used as a rule of thumb to convert the MSS_{err} grid values into mGals (Figure 3b). The result is a qualitative indicator of the least expected gravity error in the study area, which does not include the actual error of the EGM2008 model.

2.1.2. S&S Model

The S&S data set uses the slope-to-gravity method, which is based on the same remove/restore principle as DTU13. However, in this case, the derivatives are directly computed from along-track signals, instead of the 2-D grids. The resulting slopes are interpolated and convoluted to obtain grids of W-E, S-N horizontal gravity gradients, and finally combined through the Laplace equation to obtain the vertical gravity component (Fairhead, 2016; Sandwell, 1992).

The S&S Free-air anomaly is available in a grid format with a sampling step of 1 arc-minute (Figure 3c), and it is also associated with an error grid that defines its uncertainty (Figure 3d). In this case, the error refers directly to the gravity anomaly, that is, it is expressed in mGal units, and it shows the RMS difference between (a) the slope of individual altimeter profiles and (b) the averaged grid product of W-E and S-N slope (Sandwell et al., 2014; Sandwell & Smith, 2009).

Thanks to the direct computation of gradients from along-track signals, the S&S model may preserve high frequencies better than the DTU13, although it may also amplify residual noises, that is, non-modeled gravity effects induced by waves, tides, marine currents, or by reflections from the sea bottom in shallow waters and from the nearby inland coastal areas.

2.1.3. Coastal Noise

Errors in satellite altimeter data generally increase close to the coast, where the radar footprint covers part of the inland together with the sea surface (Dawson et al., 2015). Reflections from onshore areas generate high

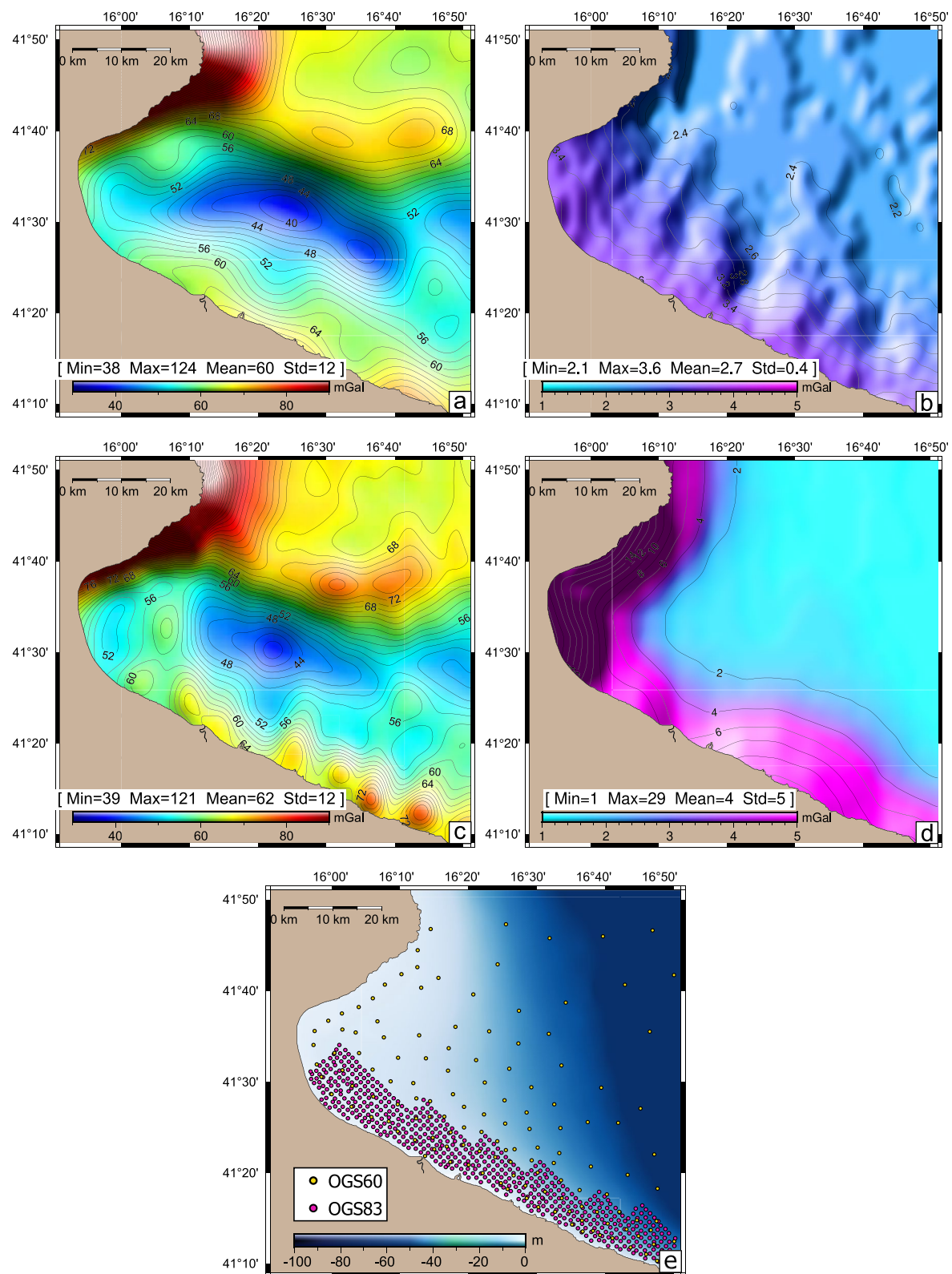


Figure 3. Free air anomaly of DTU data set with associated MSS interpolation error (a and b) and Free-air anomaly of S&S data set with associated RMS error (c and d). The error maps show how the quality of the Free-air anomaly deteriorates near the coast, up to a maximum of 29 mGal in S&S data. The lowest map (e) show the position of sea-bottom gravity stations, plotted onto the Gulf of Manfredonia bathymetry: OGS 1960 (yellow dots) and OGS 1983 (red dots).

amplitude noise covering signals reflected by the sea surface (Figures 3b and 3d). The exact distance from where this contamination may occur is not easy to estimate. It depends on a complicated combination of factors such as the angle between orbital tracks and shoreline, topographic and bathymetric gradients, and local bathymetry, and tides. This makes coastal noise a largely site-dependent problem.

Although this noise has been consistently reduced in the last few decades by using Interferometric Synthetic Aperture Radar (e.g., CryoSat2 mission), higher accuracy global gravity models (e.g., EGM2008), and more sophisticated tracking techniques, signal accuracy up to 7–14 km from the coast may still be compromised (Andersen & Knudsen, 2009; Dawson et al., 2015; Deng & Featherstone, 2006; Sandwell & Smith, 2009).

For these reasons, interpretations of altimeter-derived gravity in coastal regions must be carefully evaluated and preferably integrated with ship-borne/air-borne gravity measurements or other types of geophysical data.

2.2. Sea-Bottom Gravity Data

2.2.1. OGS60

OGS60 is part of a data set recorded during a seven-year mission (1953–1960) to extend the Italian land-based gravity network (RFI) offshore and to create the first gravity maps of the Italian seas (Ciani et al., 1960). Gravity data were measured using a Western sea-bottom relative gravimeter, with a nominal accuracy of 0.05 mGal. Station depths were measured by echo-sounders (Atlas-Werke) and coordinates calculated using optical and/or radar instruments pointing to coastal markers or reflective buoys. Planar coordinate precision decreases with increasing distance from the coast: from a minimum of ± 50 m inshore to a maximum of ± 200 m at ~ 120 km from the coast, or even up to ± 600 m when reflective buoys were not available. The OGS60 stations are not regularly distributed; station spacing increases offshore from a minimum of ~ 1.6 km to a maximum of ~ 10 km at 60–70 km from the coast (Figure 3e).

2.2.2. OGS83

OGS83 data were collected in 1982 as part of a 98-day marine gravity survey, commissioned by the Agip Mineraria company, to create high-resolution gravity maps of the Adriatic coast from Ancona to Ortona (the "northern zone"), and from Manfredonia to Brindisi (the "southern zone"). Gravity differences were measured with a LaCoste and Romberg sea-bottom relative meter (mod. 19 G), with a nominal accuracy of 0.05 mGal (Gantar, 1983). Station depth was measured by both echo-sounders (Honeywell ELAC, mod. LA2721 A) and pressure meters, giving a final combined accuracy of ± 0.5 m. Horizontal coordinates were calculated through radar trilateration from the coast (Motorola System) with a nominal precision of ± 3 m $\pm 0.01 \times$ distance (km). The OGS83 stations are distributed on a near regular grid up to ~ 110 km from the coast, at a distance of $\sim 1 \pm 0.2$ km from each other (Figure 3e).

3. Methods

The computation of gravity anomalies from sea-bottom data (OGS60 and OGS83) differs slightly from the procedure generally used with sea-surface data (e.g., DTU13 and S&S). A correct comparison can only be achieved when both data types are adjusted for the same disturbing effects, that is, all the gravity signals are not related to the sub-bottom target sources (Ballu et al., 1998).

To achieve this condition, we first calculate the Free-water anomaly, Fw , for the sea bottom gravity data:

$$Fw = g_{obs} - (g_{th} + fwc) \quad (2)$$

where g_{obs} is the observed gravity and fwc is the Free-water correction.

We then calculated the Bouguer anomaly of both altimeter-derived gravity and sea-bottom gravity (Ba_{sat} and Ba_{sb}) using two different solutions based on a common computational scheme to derive the total topographic effect (Te_{sat} and Te_{sb}):

$$Ba_{sat} = Fa - Te_{sat} \quad (3)$$

$$Ba_{sb} = Fw - Te_{sb} \quad (4)$$

Table 1

Statistics of Differences Between Sea-Bottom Gravity Data Sets OGS60 and OGS83 (Figure 3e)

	Min	Max	Mean	Std	RMS	Number of points
OGS83-OGS60	-0.79	1.7	0.1	0.57	0.58	59

Note. The differences are calculated on the OGS60 stations, in the overlapping area between the two data sets, by linearly interpolating the OGS83 values at the same coordinates. Unit of measurement in mGal.

where Fa is the free-air of satellite-altimetry data sets (Equation 1).

After computing the Bouguer anomaly, the OGS83 and OGS60 stations were merged into a unique data set, the OGS. The validity of this merging operation is supported by a statistical analysis of the differences between the two data sets within the overlapping near-shore area. Most of the differences are around ± 1.2 mGal, with an average bias that is negligible when compared to satellite altimeter errors (Table 1). This finding ensures a precision higher than 1 mGal for sea-bottom gravity since the repetition of measurements in two different periods over the same area gives an average discrepancy of just ~ 0.58 mGal (RMS).

As a final step, the Bouguer anomaly of sea-bottom data should have been upward continued from the drape seafloor surface to a constant mean sea level to have all data sets at the same distance from the causative sources (Ballu et al., 1998). However, since the average seafloor is at a ~ 50 m depth (mean vertical step) and most of gravity stations are spaced ~ 1 km (smallest horizontal step), the upward-continuation amplitude would have been lower than 1 mGal and likely affected by numerical noise. We therefore decided to skip this last processing step.

3.1. Theoretical Gravity (g_{th})

The theoretical gravity, g_{th} , was calculated using the WGS84 ellipsoid as a reference model (Decker, 1986), that is, the same used for satellite altimetry. The WGS84 model includes the mass of the atmosphere above the reference surface and the total mass of the solid Earth. The effect of the atmospheric layer must then be removed from the theoretical gravity since the net gravitational force exerted by outer spherical shells on any point inside is zero (Hinze et al., 2005):

$$g_{th}(\lambda) = \frac{978032.67714 (1 + 0.001931851386 \sin^2 \lambda)}{(1 - 0.00669437999013 \sin^2 \lambda)^{1/2}} - g_{atm} \quad (5)$$

where λ is the geographic latitude and g_{atm} is the value for atmospheric correction at the sea level, that is, 0.87 mGal.

3.2. Free-Water Anomaly (f_{wc})

The theoretical gravity of stations located below the water masses was corrected for the relative depth of each measurement point, using the free-water correction f_{wc} (Ballu et al., 1998; Dubois & Deplus, 1989; Hildebrand et al., 1990; Luyendyk, 1984; Stacey & Tuck, 1981):

$$\begin{aligned} f_{wc}(h) &\simeq \frac{\partial (g_{th}^s - g_{shell})}{\partial r} h \\ &\simeq -\frac{2 g_{th}^s}{R^2} h + 4\pi G \rho_w h \\ &\simeq -0.222 h \end{aligned} \quad (6)$$

where h is the station depth ($h \leq 0$), ρ_w is the water density ($1,030 \text{ kg m}^{-3}$), g_{shell} is the downward attraction of a homogeneous spherical shell, and G is the gravitational constant ($6.67 \times 10^{-11} \text{ m}^3 \text{s}^{-2} \text{kg}^{-1}$).

The free-water correction is similar in principle to the atmospheric correction: the water layer overlying the measurement point approximates the outermost homogeneous spherical shell of the reference model, which has a null gravity effect on the inner region. As a result, the total downward gravitational attraction of the theoretical model slightly decreases with depth because of the lack of mass contribution from the thickening outer shell. This effect is in contrast to the more significant increment in the gravitational attraction due to the closer proximity of the Earth-mass center. The combination of both effects is a slight decrease of the vertical gravity gradient by a quantity approximately equal to the gravitational attraction of the water shell (Equation 8).

The homogenous-spherical shell approximation holds if (a) the density does not change drastically within the water column and (b) the effect of Earth curvature is negligible (Bullard, 1936). The study area fills both

conditions since it is smaller than 200 km and the water layer is on average \sim 50 m. Otherwise, the ellipsoidal-shell approximation and water-density profiles should have been included in the computation (Stacey & Tuck, 1981).

3.3. Topographic Effect (Te)

The gravity effect of topographic and water masses in the Bouguer anomaly (Equations 3 and 4) was computed differently in the case of sea-bottom and sea-surface gravity data since the respective computational points are at different vertical levels to the reference ellipsoid. Then, according to the Poincare-Prey reduction theory, the gravitational attraction of water and landmasses surrounding the sea-bottom stations is consequently different from that of any point above them (Hofmann-Wellenhof & Moritz, 2006).

In both cases, the adopted computational scheme separately considers the effect of (a) a high-resolution Digital Topographic-Bathymetric Model (DTBM) with a grid step of 100 m, extended for 9 km from the computational point, and (b) the effect of a low-resolution DTBM, with a 3 km grid-step which extends for 159 km from the limits of the high-resolution area.

The DTBM was created by combining the SRTM and the EMODnet models, and then, converted into a list of 3-D prisms (EMODnet Bathymetry Consortium, 2018; Farr & Kobrick, 2000). The gravity effect of each prism is calculated through the Python library Harmonica (Uieda et al., 2020), which makes use of the analytical solution proposed by Nagy et al. (2000). This solution has the advantage of being valid on any point, either outside or inside the prism (Fukushima, 2019; Nagy et al., 2002).

3.3.1. Topographic Effect at the Sea-Surface (Te_{sat})

When the measurement point lies on the sea surface (as for altimeter-derived gravity), the reference model must be corrected for effects of crustal masses above the point and water masses below it in order to obtain the complete Bouguer anomaly (Figures 4a and 4b).

We therefore calculated the topographic effect, Te_{sat} , by summing (a) the vertical upward attraction of crustal masses above the reference surface (Zone A), and (b) the drop in the gravitational attraction due to the presence of water in place of the crust in marine areas (Zone B). In this computation, we used the constant density of 2.67 g/cm³ for the crust, ρ_c , and 1.03 g/cm³ for the water density, ρ_w .

This approximation may vary locally because of inland depressions (continental areas below the reference surface) or inland water masses (e.g., large lakes or lagoons).

The solution is identical for measurement points above the reference surface (e.g., land-based stations or air-borne measurements). The difference is that the attraction of topographic masses may be either positive or negative, depending on the height of the computational point relative to the surrounding topography.

$$\left\{ \begin{array}{ll} \text{Zone}(A) : g_e(h, 0, \rho_c) & \text{if } h > 0 \\ \text{Zone}(B) : g_e(0, h, \rho_w - \rho_c) & \text{if } h < 0 \end{array} \right\} \quad (7)$$
$$Te_{sat} = \sum_A g_e(h_t, h_b, \rho) + \sum_B g_e(h_t, h_b, \rho)$$

where g_e is the gravitational attraction of a prism, with h_t and h_b being the top and the bottom height of the element, respectively, and h the height given by the DTBM model.

3.3.2. Topographic Effect at the Sea-Bottom (Te_{sb})

We assumed in Equation 5 that the starting reference model is a layered sphere (Figure 4c). In this approximation, the outermost layer above sea bottom stations is made of water with a constant density; hence, it has a total null gravity effect on any point inside. However, both water and crustal masses are non-homogeneously distributed above the stations in the real model (Figure 4d).

Therefore, the gravity effect of all the heterogeneously distributed masses above the computational point must be added as an upward attraction to the theoretical gravity (i.e., negative effect). The remaining effects of the water

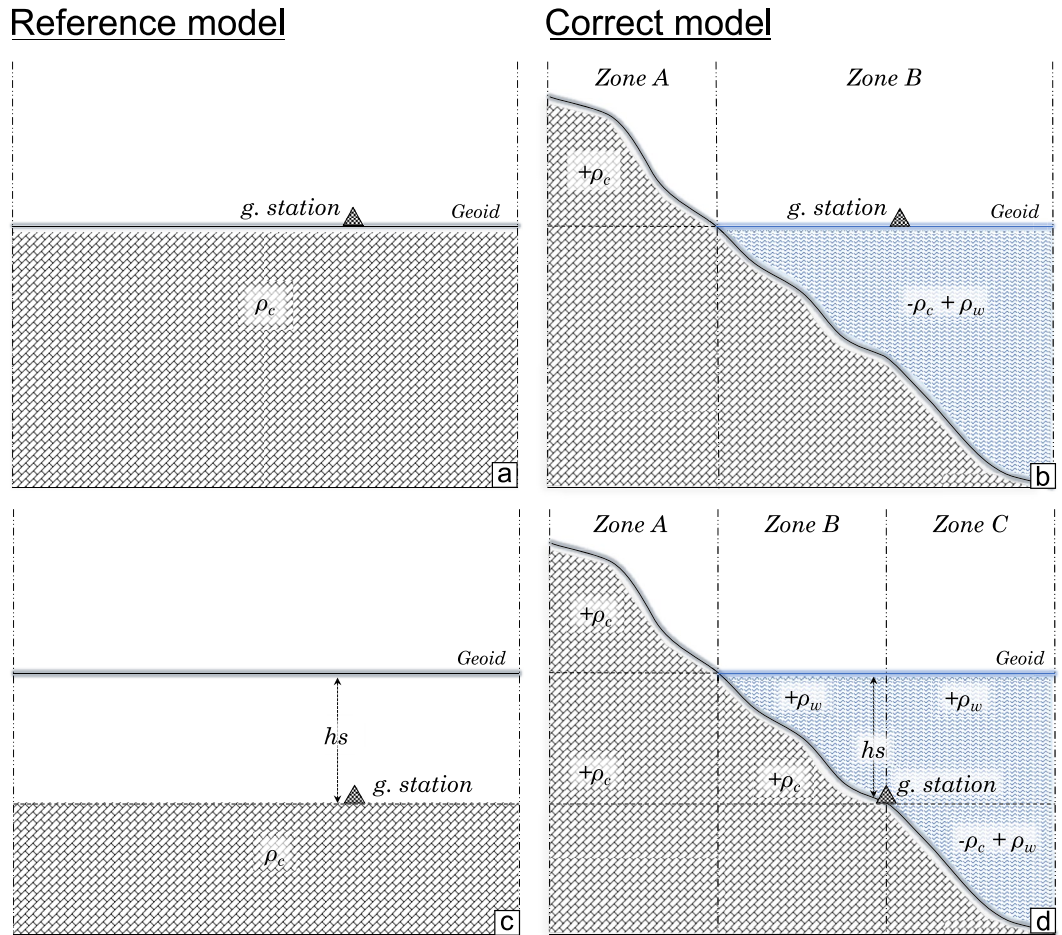


Figure 4. Schematic representation of models used to compute the topographic effects of sea-surface gravity ([a, b], Equation 7) and sea bottom gravity ([c, d], Equation 8). On the left, the reference model, and on the right, the correct model including all the density corrections that must be added to the reference model in order to come to a correct estimate of the topographic effect.

masses below the computational point (Zone C, Figure 4d) should be treated like those of sea-surface stations, that is, by removing the crustal effect and adding back the effect of the water (Equation 8).

The problem is solved by dividing the DTBM model into three zones (Gantar, 1983; Nowell, 1999):

$$\begin{cases} \text{Zone}(A) : g_e(h, h_s, \rho_c) & \text{if } h > 0 \\ \text{Zone}(B) : g_e(0, h, \rho_w) + g_e(h, h_s, \rho_c) & \text{if } h_s < h < 0 \\ \text{Zone}(C) : g_e(0, h_s, \rho_w) + g_e(h_s, h, \rho_w - \rho_c) & \text{if } h < h_s < 0 \end{cases} \quad (8)$$

$$Te_{sb} = \sum_A g_e(h_t, h_b, \rho) + \sum_B g_e(h_t, h_b, \rho) + \sum_C g_e(h_t, h_b, \rho)$$

where h_s is the depth of the computational point (i.e., negative height).

3.4. Field Derivatives

Gravity field derivatives are commonly used in geophysical studies to enhance lateral density contrasts at depth (Aydogan, 2011; de Lerma et al., 2015; Fedi & Florio, 2001). The multiscale derivative has already proven helpful in identifying the offshore continuation of the Mattinata Fault system (the "Gondola ridge") in larger scale

regional analyses (Fedi et al., 2005). In this study, we use the ISVD and the Tilt derivative (Fedi, 2002; Fedi & Florio, 2001; Miller & Singh, 1994), for a qualitative evaluation of the sensitivity to lateral density contrast of each different gravity data set (DTU, S&S, OGS). The ISVD was calculated in three steps (Fedi & Florio, 2001): (a) integrating the gravity anomaly grid within the frequency domain, (b) computing the second-order horizontal derivatives in the space domain using a 2D convolution, and (c) calculating the first-order vertical derivative combining the results from the previous step through the Laplace equation.

The Tilt derivative is the angle given by the ratio between the ISVD and the first-order horizontal gravity gradient, which is also computed through a spatial-domain convolution:

$$\text{Tilt} = \text{atan} \left[\frac{\text{ISVD}}{\sqrt{\left(\frac{\partial g}{\partial x} \right)^2 + \left(\frac{\partial g}{\partial y} \right)^2}} \right] \quad (9)$$

where g is the gravity anomaly and the denominator is the total horizontal gradient.

The calculated functions have been qualitatively evaluated by direct comparison with a forward gravity model. This model includes the interface between the Oligocene Quaternary sediments and the underlying carbonate platform, as per Volpi et al. (2015), in which depths were derived from a 2D inversion of multichannel seismic profiles constrained by well-log data. The gravity effect of the seismic interface is computed using the Parker method in the FFT domain (Parker, 1973):

$$\Delta g(x, y) = \text{FFT}^{-1} \left\{ -2\pi G \Delta \rho e^{-h_0 |\vec{K}|} \sum_{n=1}^{\infty} \frac{|\vec{K}|^{n-1}}{n!} \text{FFT} [h(x, y)^n] \right\} \quad (10)$$

where Δg is the gravity effect of the 2D interpreted seismic layers, depth-converted, h is the depth of the layer, $\Delta \rho$ is density contrast between the two layers forming the interface, h_0 is the mean depth of the interface, and \vec{K} is the wavenumber.

A first-order polynomial surface was removed from the Bouguer anomaly before computing the derivatives in order to take out the regional component of the gravity field.

We considered the linear trend surface to be an acceptable approximation for the regional gravity effects, under the assumption that over the Italian territory both the Moho and the crystalline basement have wavelengths longer than 100 km (Corrado & Rapolla, 1981), and our study area is less than 90 km in extent.

The Tilt function allowed us to map the edges of the gravity sources using the residual gravity field. Lines approximating these edges were outlined through a maximum detection algorithm built using a 3×3 km moving window operator (Blakely & Simpson, 1986). The operator slides on the cosine of the Tilt, also known as the Theta derivative. The Theta derivative is always positive and has its maximum values, that is, the zero Tilt values correspond with sub-surface lateral discontinuities (Fairhead, 2016; Wijns et al., 2005). The ridge axis of the Gondola system was calculated in the same way but using the Tilt function instead of the Theta function because it shows maximum values immediately above the top-center of the causative sources. The detected edges were divided into two sets: the first containing lines correlating with fault interpretation based on seismic profiles or with visible changes in the trend of a carbonate platform (verified edges); and a second containing lines only registered by gravity (inferred edges). The “gravity edges” combine the results from the OGS data within a coastal strip of ~ 17 km and the S&S data in the remaining areas.

4. Results and Discussion

The Bouguer anomaly values follow an approximately bimodal distribution (Figure 5a). The first mode, centered at 60 mGal, represents the near-shore area southwest of the Gondola fault system. The second mode, at 75 mGal, accounts for values covering the north-eastern sector, with relatively higher positive values than those in the area to the southwest. The differences between the two sectors are mainly related to the abrupt discontinuity of the

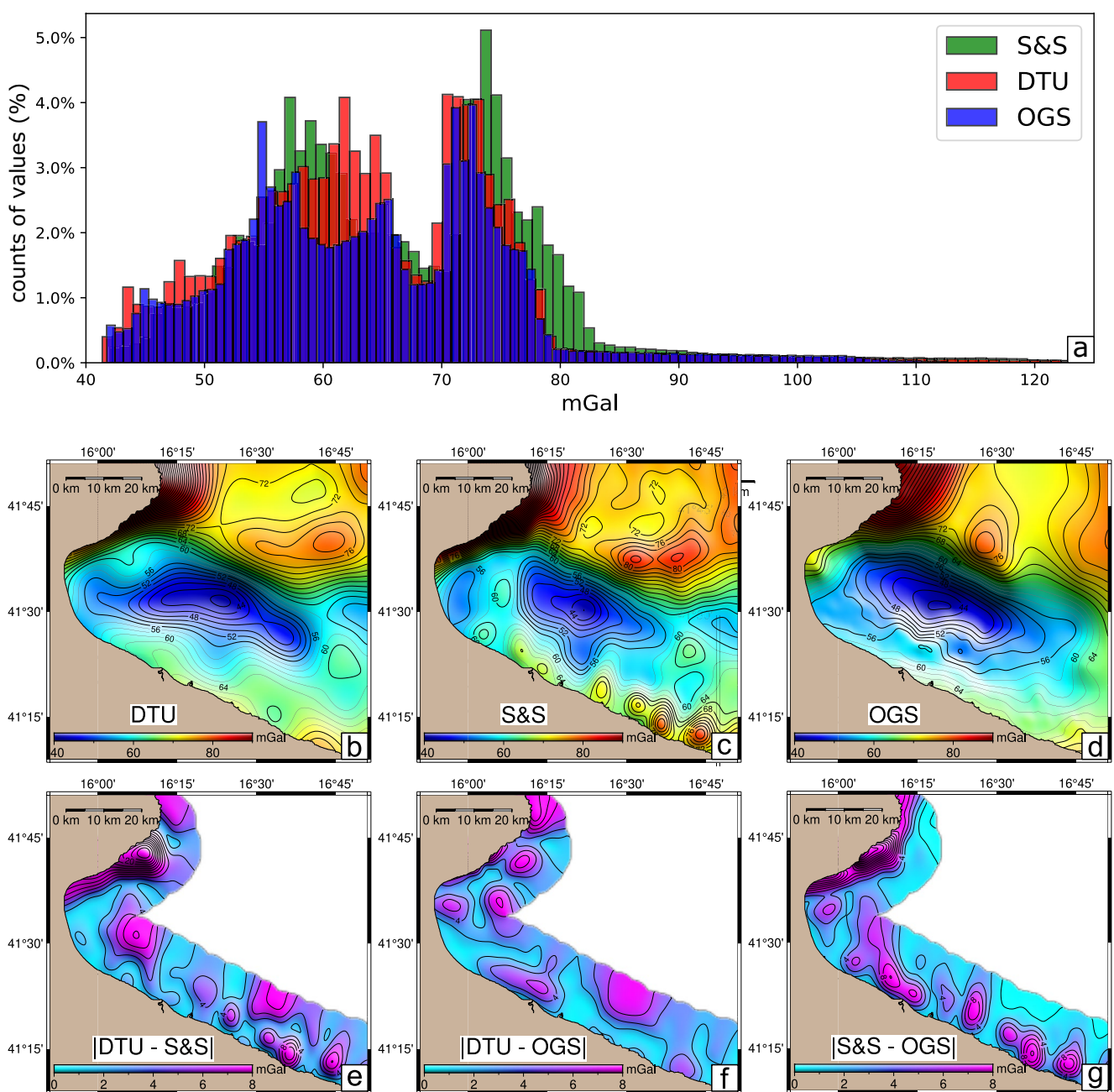


Figure 5. Distribution of Bouguer anomaly values (a), Bouguer anomaly maps (b–d) and relative absolute differences of DTU, S&S, OGS data sets (e–g). A block mean average, with ~ 2 km window size, and low-pass Gaussian filter, with a 6 km window size, have been used to avoid aliasing errors (Wessel et al., 2019) and to bring all data sets to the same empirical lowest resolution. The differences are mapped within a 15 km wide coastal strip, which is the area mostly affected by coastal noise in satellite data and, at the same time, densely covered by the OGS sea-bottom stations. The absolute value stresses the total magnitude of differences, without the bias of the sign. The coastal noise is easy to identify in the S&S data set and in the S&S-OGS differences, where it forms a sort of “ringing effect” up to ~ 17 km seaward.

Gondola Fault Zone. The fault corresponds with a break in the main regional gravity trend associated with wavelengths of ≤ 200 km. The same discontinuity extends to the north over the Gargano Peninsula, along with the Mattinata Fault, and it is also visible in the magnetic data (Fedi et al., 2005). Since regional gravity signals are likely to be related to crustal discontinuities, for example, the crystalline basement and/or the Moho (Corrado & Rapolla, 1981), the presence of a nearly vertical step of ~ 30 mGal breaking the continuity of the main Bouguer

Table 2

Statistic of the Bouguer Gravity Anomaly Calculated for Each Data Set (DTU, OGS, and S&S), and Relative Differences Within a 17 km Wide Coastal Strip (DTU-S&S, DTU-OGS, DTU-OGS)

	Min	Max	Mean	Std	RMS	Number of points
DTU	41.04	124.49	64.18	11.73	-	1,739
S&S	41.78	123.87	66.46	12.01	-	1,739
OGS	41.43	102.77	60.58	6.58	-	671
DTU-S&S	-27.33	7.11	-2.89	6.21	6.86	333
DTU-OGS	-20.47	19.18	1.17	4.07	4.23	333
S&S-OGS	-6.99	38.57	4.07	6.66	7.8	333

Note. The differences are calculated on regular grids with 2.5 km grid-step. Unit of measurement in mGal.

trend may suggest that the base of the fault system is much deeper than the Jurassic layer, which is around a depth of 2–3 km (Volpi et al., 2015).

The relative minimum of about −30 mGal near the western coast extends for ~30 km in the SW–NE direction, ~50 km in the NW–SE direction, and it has a similar amplitude and shape in all the data sets that have been studied (DTU, S&S, and OGS). Based on the information gathered from seismic reflection data, we assert that part of this residual anomaly is related to a local sedimentary basin reaching depths of ~1,500 m.

The Bouguer anomaly values from the DTU model show approximately the same statistical information and similar spatial distribution as the S&S (Table 2 and Figures 5b and 5c). However, the S&S model has higher amplitudes and shorter wavelengths than the DTU, as shown in the data distribution and by the map of data differences (Figures 5a and 5e). The S&S data register short-wavelength anomalies near the SE coast, ~6 km wide, which occur as a “ringing effect” and can reasonably be expected to be caused by the radar signals reflected from adjacent land areas, that is, coastal noise

(Figure 5c). The noise degrades the S&S gravity anomaly up to ~17 km from the coast. This is approximately the size of the most prominent positive anomaly in the SE coastal sector of the study area, calculated as the distance from the coast to the first zero value in the ISVD map (Figure 6h).

Differences between the OGS and satellite altimeter data sets (DTU and S&S) show values greater than 15 mGal in the vicinity of the NW coast (i.e., the Gargano Promontory). In this area, significant positive differences correlate with high topographic gradients (Figures 5e–5g). However, this coastal area is also poorly covered by sea-bottom stations (more than 6 km apart), which means differences may also be caused by interpolation artifacts rather than coastal noise. The absolute value of differences between the satellite altimeter gravity and the OGS sea-bottom data (Table 2) is approximately within the estimated satellite altimeter errors (Andersen et al., 2014; Sandwell et al., 2014). Nevertheless, the maximum and minimum differences are greater than 20 mGal, meaning that the satellite altimeter grids in coastal areas contain outliers that are a few tens of mGals higher than the predicted uncertainties if considering sea-bottom gravity as a correct reference.

After removing a first-order linear trend, the residual anomaly (Figures 6a, 6d and 6g) should correlate with the carbonate basement, that is, it should respond mainly to the density contrast between carbonate rocks and the overlying terrigenous sequence (Corrado & Rapolla, 1981; Fedi & Rapolla, 1993; Rapolla, 1986). This hypothesis is partially confirmed by the forward gravity model based on seismic reflection data, which shows patterns similar to the observed residual gravity. However, amplitudes of residual gravity on the Gondola ridge are almost ~10 mGal higher than the calculated gravity (Figure 7a), which may reinforce the hypothesis of a deeper origin than the Jurassic sequence for the base of this Gondola System.

The residual gravity, the ISVD, and the Tilt maps (Figure 6) provide further evidence that S&S contains higher frequencies than the DTU model: it has both the highest ringing noise near the coast and the sharpest gravity gradient corresponding to the Gondola ridge, as highlighted by the forward gravity model. Furthermore, the ISVD of S&S data correlates positively with the ridge axes. In addition, the data set resolution allows us to map the slight change in the main ridge axis orientation from NW–SE to E–W, which is less evident in both the DTU and OGS data. This confirms that, of the data sets investigated, the S&S is the most accurate away from the coast and, at the same time, the noisiest in near-shore areas. On the other hand, the OGS data are the most reliable near coasts where there is an almost regular distribution of sea-bottom stations that are separated by distances of ~1 km, and do not register any evident systematic bias between data acquired in subsequent surveys (Figures 3e and Table 1).

The ISVD map of OGS data shows local relative minima close to the coast, with sizes ranging from 5 to 6 km (Figure 6b). Each of these minima is covered by more than three gravity stations, and they are not related to any local structural discontinuity as shown by seismic reflection profiles on the top of the carbonate layer, which appears to be relatively flat in this sector. Excluding the presence of localized deeper sources and/or measurement biases, these small gradient changes may be related to localized variations within the Pliocene and Pleistocene sediments (D. Morelli, 2002; Volpi et al., 2015). As described in the geological setting above, at least two different

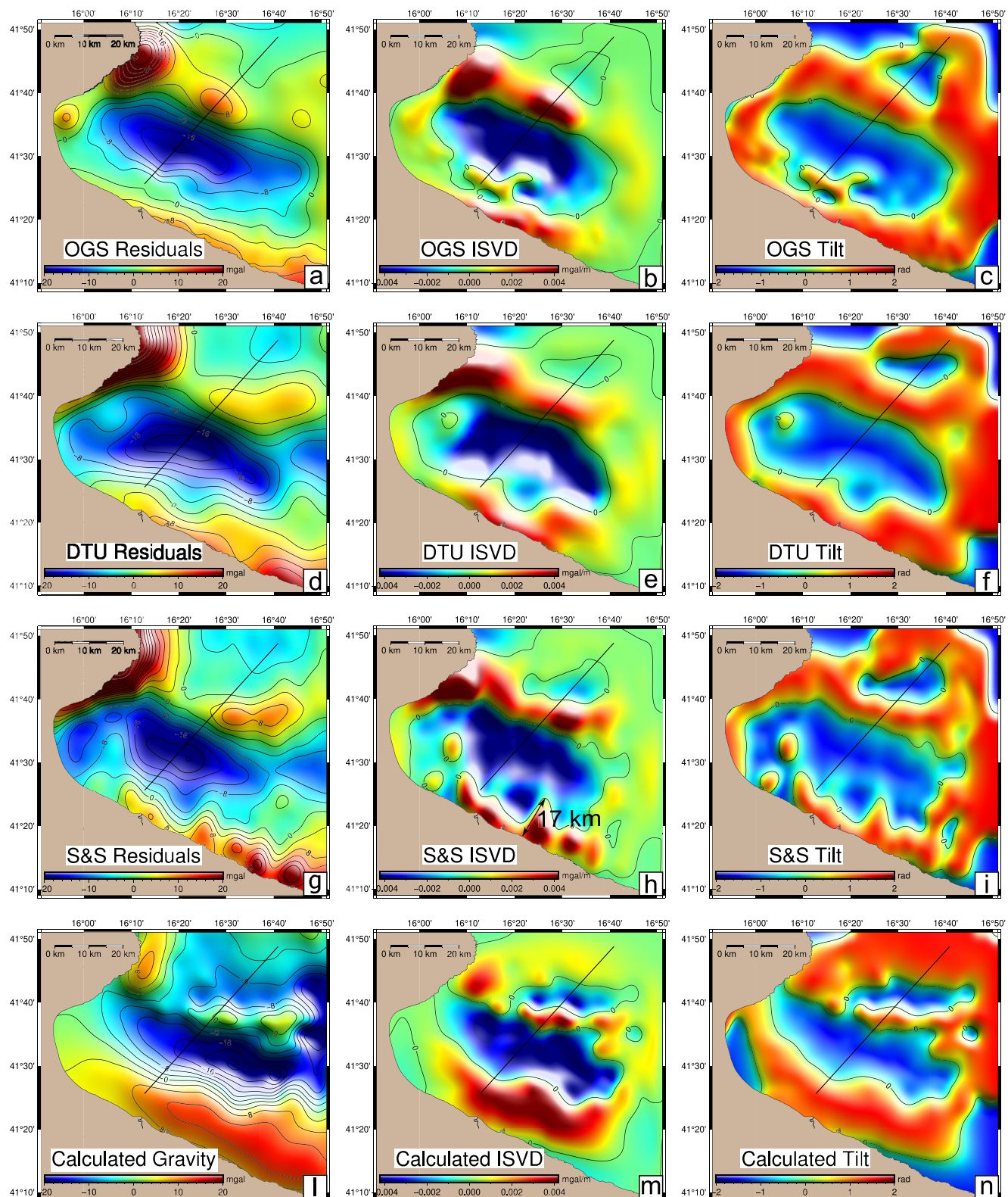


Figure 6. The subplots show, from left to right, (i) the observed gravity residuals, (ii) the Integrated Second Vertical Derivative (ISVD), and (iii) the Tilt function of OGS (a–c), DTU (d–f) and S&S (g–i) data sets. The bottom plots (l–n) show the calculated gravity effect of the 2D depth interface, obtained from depth-converted seismic reflection data, which separates sedimentary deposits from carbonate rocks. The black line indicates the profile analyzed in Figure 7.

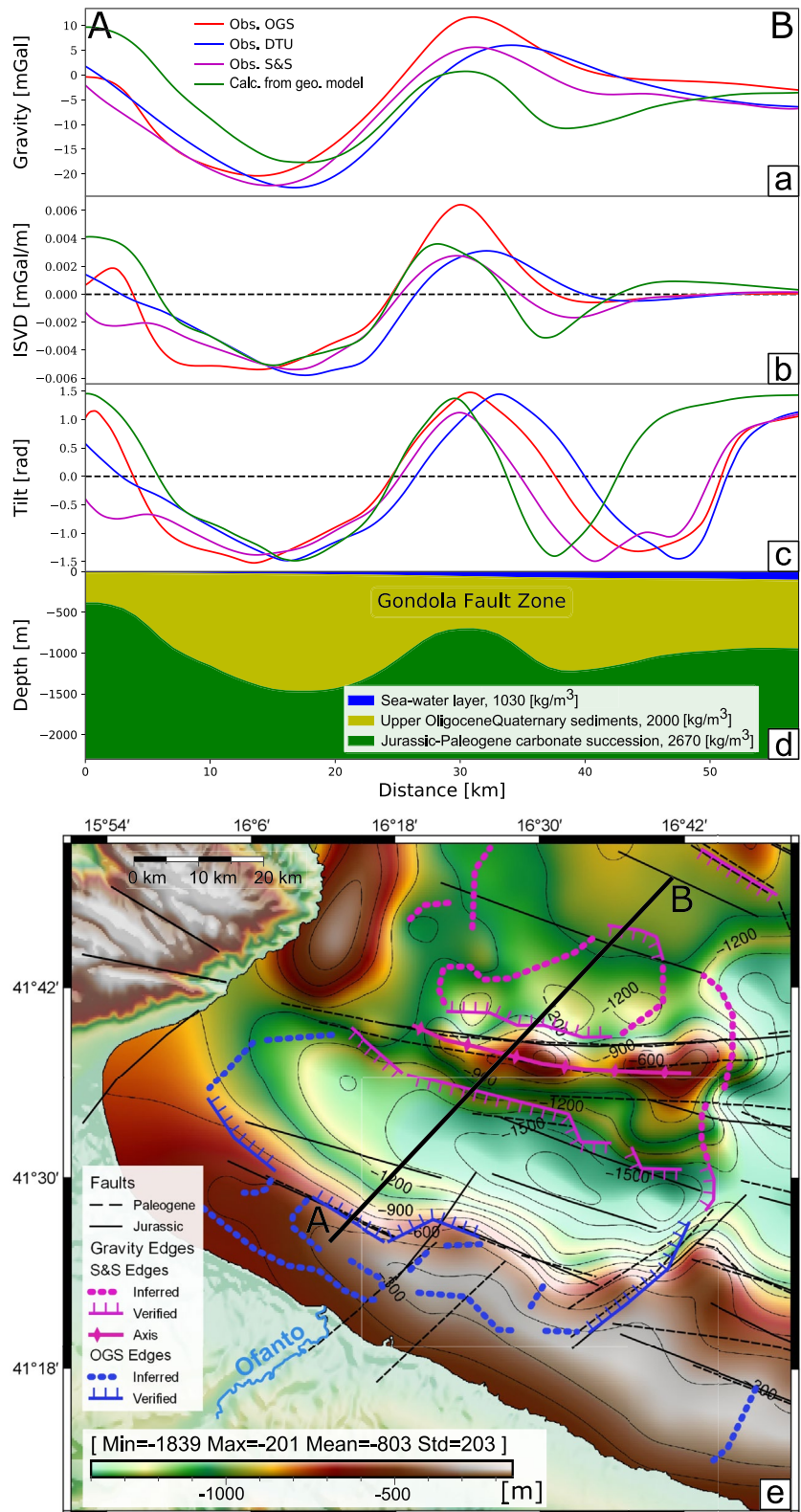


Figure 7.

sedimentary units have been recognized from the interpretation of seismic profiles (Figure 2b): the upper unit is composed of Plio-Quaternary siliciclastic sediments, which we assumed are less dense and less compacted than the lower Oligocene-Miocene unit composed of silico-clastic and calcareous turbidites (Volpi et al., 2015). The normal superposition of these units has been hypothesized to have been locally modified by tectono-eustatic processes (D. Morelli, 2002) and probably by different sedimentary river inputs and erosion mechanisms, leading to lateral depositional transitions (heterotopic facies). The ISDV map (Figure 6b) shows that one of the relative minima is located directly in front of the mouth of the Ofanto (Figure 7e), the largest river in the Puglia region, which transports and deposits a considerable amount of sediments into the sea (Mastronuzzi et al., 2002). If confirmed, this hypothesis could be an important proof of the capabilities of the Italian sea-bottom gravity network to distinguish even small density variations within sedimentary bodies, which may be extremely useful in the absence of seismic profiles acquired near the coast.

The ISVD and the Tilt derivatives enhance lateral density transitions. In both functions, the zero value marks the approximate edges of causative sources, that is, lateral discontinuities of subsurface interfaces. The Tilt, unlike ISVD, is normalized between $\pm \pi/2$, and it tends to saturate faster over bodies with relatively higher densities with respect to the surroundings. This property makes the Tilt derivative particularly useful when outlining the planar shape of the carbonate platform, as imaged by gravity maps (Figure 7).

All the data sets investigated show similar results for the positioning of the SW edge of the Gondola ridge. However, they do not have sufficient resolution and perhaps lack the necessary accuracy to outline the ridge's NE side correctly. On the NE margin, the shape of the gravity anomaly over the graben is smoother than on the SW side, and the residual anomaly is ~ 5 km larger than the anomaly calculated from the geological model. In this area, the OGS sea-bottom stations are separated by distances ranging from 6 to 10 km (Figure 3e). As a result, the observed gravity can not fit with the forward model, which assumes a regular distribution of the stations (i.e., 1 st/km²). The NE side of the ridge is instead better approximated by the Tilt function derived from the S&S model (Figure 7c).

South of the Gondola ridge, the gravity edges approximately correspond to the Jurassic faults as interpreted from seismic data (D. Morelli, 2002). In addition, the central axis of the ridge derived from gravity well data correlates with the pre-existing seismic interpretation (D. Morelli, 2002; Volpi et al., 2015). This confirms that part of the information contained in both the sea-bottom and satellite-altimetry gravity represents a 3D sub-surface fault network (Fairhead, 2016; Fedi & Florio, 2001; FitzGerald & Milligan, 2013). The remaining signals are associated with lateral density contrasts not necessarily related to sub-vertical steps in the rock basement (Figure 7e). For example, in the north-eastern part of the map, the “gravity edges” extracted from the S&S data appear to outline smooth variations of the bedrock surface rather than abrupt discontinuities.

Other “gravity edges” derived from OGS sea-bottom data contour local minima near the coast. These edges correlate with SW-NE-oriented Paleogene faults cutting the southern shoreline sector (Figure 7e). These lineaments are Dinaric transfer faults, which reactivate an older NE-SW Jurassic horst-graben system (D. Morelli, 2002). The reactivation dislocates the Oligocene-Miocene deposits, creating a lateral transition with the upper sedimentary unit, which supposedly has a lower density.

5. Conclusions

In this study, sea-bottom gravity measurements (OGS) have been compared with sea-surface satellite altimeter-derived gravity (DTU and S&S) in the Gulf of Manfredonia.

All the gravity data types investigated, once corrected for effects of the free-water gradient and topographic/water masses, show statistical comparability and spatial correlation in the imaging created from this gravity anomaly data. All data sets show the same negative anomaly associated with a $\sim 1,500$ m deep basin located immediately

Figure 7. Representative depth profile of the geological model derived from seismic interpretation, crossing the Gondola Fault Zone (d). Upper panels (a–c) show the trend of the observed residual gravity, the ISVD, and the Tilt functions, calculated for each different data set (OGS, DTU, and S&S) and for the geological model. The zero values of both ISDV and Tilt mark the approximate upper edges of the carbonate platforms. The bottom map (e) shows results from the edge-detection analysis, which combines OGS data up to 17 km from the coast and S&S data in the remaining areas. The gravity edges have been divided into two sets: the first set contains lines correlating with the general trend of the faults (verified edges) and the second set contains lines only recorded by gravity (inferred edges). The ridge axis outlines the approximate top center of the Gondola ridge. The rock/sediment interface is imaged and contoured onto the offshore areas (Volpi et al., 2015). Jurassic-Paleogene faults are both based on seismic interpretations taken from previous works (D. Morelli [2002], and references therein).

to the south of the Gondola Fault Zone. The residual gravity, ISVD, and Tilt functions register the effects of the central carbonate ridge as outlined by the seismic reflection profiles.

A comparison with the forward gravity model obtained from seismic interpretation shows that the S&S data set allows more accurate identification of the lateral sediment/rock transition when compared to the other gravity data sets (i.e., DTU and OGS). However, S&S is severely compromised by coastal noise up to 17 km from the shoreline, where the interpretation of residual gravity is highly inconsistent. The DTU data set shows a lower high-frequency content than S&S data, despite being less noisy near the shore.

The combined interpretation of the OGS sea-bottom and altimeter-derived gravity data allowed the edges of the carbonate platform to be mapped with a high degree of confidence both near and further away from the coast. Part of the gravity-derived edges correlate with faults within the Gondola Fault Zone that have been detected by seismic profiles. Other edges mark the smooth transition between rock and sediments rather than abrupt discontinuities generated by faults. Some edges, detected only by sea-bottom gravity data near the eastern coast, outline shallow anomalies with low amplitudes, which could be related to relatively small density contrasts in the river deposits and/or differential sediment compaction. In a few cases, these near-shore edges also seem to be partially related to SW-NE-oriented lateral discontinuities, as identified by seismic data. This finding shows how the high-resolution sea-bottom gravity network around the Italian coast contains information about sub-surface geological structures not fully detectable by satellite altimetry or the available seismic data.

The comparative analysis described here shows the effectiveness of coupling information from sea-bottom and satellite altimeter-derived gravity to reduce uncertainties of altimeter signals in localized coastal areas. In particular, the results help to outline and better image geological structures propagating from inland toward the offshore areas of the Salento region with greater accuracy than possible when using only a single gravity or seismic data set.

Data Availability Statement

The S&S data set is available through Sandwell et al. (2014), at <https://www.earthbyte.org/new-global-marine-gravity-model-sandwell-et-al-2014>. The DTU13 data set is available through Andersen et al. (2013) at <https://ftp.space.dtu.dk>. For the topographic corrections, we used the Python library Harmonica, which is part of the project Fatiando a Terra (Uieda et al., 2020), available at <https://www.fatiando.org>.

Acknowledgments

All grid files and maps were created using Generic Mapping Tools (GMT) version 6.1.1. The multichannel seismic-reflection data comes from the project ViDEPI (Visibility of Petroleum Exploration Data in Italy), managed by the Italian Ministry of Economic Development, and made available in SEG-Y format on the SNAP (Seismic Data Network Access Point) platform managed by the Istituto Nazionale di Oceanografia e Geofisica Sperimentale (Diviacco, 2018). The authors thank ENI for kindly providing the sea-bottom gravity data set OGS83 (Gantar, 1983). The OGS sea-bottom gravity data set is part of the OGS gravity database (Ciani et al., 1960; C. Morelli, 1966). The DTBM is a combination of SRTM and EMODnet data. The SRTM product is released by the National Aeronautics and Space Administration (NASA) and downloaded from the USGS EROS Data Center, courtesy of the U.S. Geological Survey. The EMODnet product is provided by the EMODnet Bathymetry Consortium (2018): EMODnet Digital Bathymetry (DTM).

References

- Andersen, O. B. (2013). Marine gravity and geoid from satellite altimetry. In *Geoid determination* (pp. 401–451). Springer. <https://doi.org/10.1007/978-3-540-74700-9>
- Andersen, O. B., & Knudsen, P. (1998). Global marine gravity field from the ERS-1 and Geosat geodetic mission altimetry. *Journal of Geophysical Research*, 103(C4), 8129–8137. <https://doi.org/10.1029/97JC02198>
- Andersen, O. B., & Knudsen, P. (2000). The role of satellite altimetry in gravity field modelling in coastal areas. *Physics and Chemistry of the Earth, Part A: Solid Earth and Geodesy*, 25(1), 17–24. [https://doi.org/10.1016/S1464-1895\(00\)00004-1](https://doi.org/10.1016/S1464-1895(00)00004-1)
- Andersen, O. B., & Knudsen, P. (2009). The DNSC08 mean sea surface and mean dynamic topography. *Journal of Geophysical Research*, 114, C11. <https://doi.org/10.1029/2008JC005179>
- Andersen, O. B., Knudsen, P., Berry, P., Freeman, J., Pavlis, N., & Kenyon, S. (2008). *The DNSC08 ocean wide altimetry derived gravity field: EGU Meeting Programme*. Abstract EGU2008-A-07163, G1-1MO10-003.
- Andersen, O. B., Knudsen, P., & Berry, P. A. M. (2010). The DNSC08GRA global marine gravity field from double retracked satellite altimetry. *Journal of Geodesy*, 84(3), 191–199. <https://doi.org/10.1007/s00190-009-0355-9>
- Andersen, O. B., Knudsen, P., Kenyon, S., Factor, J., & Holmes, S. (2013). The DTU13 global marine gravity field—First evaluation. In *Ocean Surface Topography Science Team Meeting*, Boulder, CO.
- Andersen, O. B., Knudsen, P., Kenyon, S., & Holmes, S. (2014). Global and arctic marine gravity field from recent satellite altimetry (DTU13). In *Paper presented at 76th EAGE Conference and Exhibition 2014* (Vol. 2014, pp. 1–5). <https://doi.org/10.3997/2214-4609.20140897>
- Andersen, O. B., Knudsen, P., & Stenseng, L. (2015). The DTU13 mss (mean sea surface) and MDT (mean dynamic topography) from 20 years of satellite altimetry. In *IGFS 2014* (pp. 111–121). Springer. https://doi.org/10.1007/1345_2015_182
- Aydogan, D. (2011). Extraction of lineaments from gravity anomaly maps using the gradient calculation: Application to Central Anatolia. *Earth Planets and Space*, 63(8), 903–913. <https://doi.org/10.5047/eps.2011.04.003>
- Ballu, V., Dubois, J., Deplus, C., Diament, M., & Bonvalot, S. (1998). Crustal structure of the Mid-Atlantic Ridge south of the Kane Fracture Zone from seafloor and sea surface gravity data. *Journal of Geophysical Research*, 103(B2), 2615–2631. <https://doi.org/10.1029/97JB02542>
- Barthelmes, F. (2009). *Definition of functionals of the geopotential and their calculation from spherical harmonic models: Theory and formulas used by the calculation service of the International Centre for Global Earth Models (ICGEM)*. Retrieved from <http://icgem.gfz-potsdam.de>
- Billi, A., Gambini, R., Nicolai, C., & Storti, F. (2007). Neogene-Quaternary intraforeland transpression along a Mesozoic platform-basin margin: The Gargano fault system, Adria, Italy. *Geosphere*, 3(1), 1–15. <https://doi.org/10.1130/GES00057.1>

- Blakely, R. J., & Simpson, R. W. (1986). Approximating edges of source bodies from magnetic or gravity anomalies. *Geophysics*, 51(7), 1494–1498. <https://doi.org/10.1190/1.1442197>
- Bullard, E. C. (1936). Gravity measurements in east Africa. *Philosophical Transactions of the Royal Society of London - Series A: Mathematical and Physical Sciences*, 235(757), 445–531.
- Ciani, A., Morelli, C., & Gantar, C. (1960). Rilievo gravimetrico sullo zoccolo epicontinentale dei mari Italiani. *Bollettino di Geofisica Teorica ed Applicata*(6), 101.
- Colantoni, P., Tramontana, M., & Tedeschi, R. (1990). Contributo alla conoscenza dell'avampaese apulo: Struttura del Golfo di Manfredonia (Adriatico meridionale). *Giornale di Geologia*
- Corrado, G., & Rapolla, A. (1981). The gravity field of Italy: Analysis of its spectral composition and delineation of a tridimensional crustal model for central-southern Italy. *Bollettino di Geofisica Teorica ed Applicata*, 23(89), 17–29.
- Dawson, G. J., Green, C. M., & Fletcher, K. M. (2015). Using the SAR mode from CryoSat-2 to improve satellite derived gravity near the coast. In *Paper presented at 77th EAGE Conference and Exhibition 2015* (Vol. 2015, pp. cp–451). <https://doi.org/10.3997/2214-4609.201412985>
- de Alteriis, G. (1995). Different foreland basins in Italy: Examples from the central and southern Adriatic Sea. *Tectonophysics*, 252(1–4), 349–373. [https://doi.org/10.1016/0040-1951\(95\)00155-7](https://doi.org/10.1016/0040-1951(95)00155-7)
- de Alteriis, G., & Aiello, G. (1993). Stratigraphy and tectonics offshore of Puglia (Italy, southern Adriatic Sea). *Marine Geology*, 113(3–4), 233–253. [https://doi.org/10.1016/0025-3227\(93\)90020-V](https://doi.org/10.1016/0025-3227(93)90020-V)
- Decker, B. L. (1986). *World geodetic system 1984*. Defense Mapping Agency Aerospace Center.
- de Lerma, D., Green, C. M., Cheyney, S., & Campbell, S. J. (2015). Improved high order vertical derivatives of potential field data-extending the ISVD Method. In *Paper presented at 77th EAGE Conference and Exhibition 2015* (Vol. 2015, pp. 1–5). <https://doi.org/10.3997/2214-4609.201412755>
- Deng, X., & Featherstone, W. E. (2006). A coastal retracking system for satellite radar altimeter waveforms: Application to ERS-2 around Australia. *Journal of Geophysical Research*, 111(C6). <https://doi.org/10.1029/2005JC003039>
- Di Bucci, D., Ravaglia, A., Seno, S., Toscani, G., Fracassi, U., & Valensise, G. (2006). Seismotectonics of the southern Apennines and Adriatic foreland: Insights on active regional E-W shear zones from analogue modeling. *Tectonics*, 25(4). <https://doi.org/10.1029/2005TC001898>
- Diviacco, P. (2018). *Sismica riconoscitiva legge 613/1967 - Zona D*. OGS (Istituto Nazionale di Oceanografia e di Geofisica Sperimentale), Geophysical Section. <https://doi.org/10.6092/SNAP.580BF950A46873E44295A7E29D66F077>
- Dubois, J., & Deplus, C. (1989). Gravimetry on the Erimo seamount, Japan. *Tectonophysics*, 160(1–4), 267–275. [https://doi.org/10.1016/0040-1951\(89\)90395-8](https://doi.org/10.1016/0040-1951(89)90395-8)
- EMODnet Bathymetry Consortium. (2018). *EMODnet Digital Bathymetry (DTM 2018)*. <https://doi.org/10.12770/18FF0D48-B203-4A65-94A9-5FD8B0EC35F6>
- Fairhead, J. D. (2016). *Advances in gravity and magnetic processing and interpretation*. EAGE Publications.
- Farr, T. G., & Kobrick, M. (2000). Shuttle radar topography mission produces a wealth of data. *EOS, Transactions American Geophysical Union*, 81(48), 583–585. <https://doi.org/10.1029/e081i048p00583>
- Fedi, M. (2002). Multiscale derivative analysis: A new tool to enhance detection of gravity source boundaries at various scales. *Geophysical Research Letters*, 29(2), 16–1–16–4. <https://doi.org/10.1029/2001GL013866>
- Fedi, M., Cella, F., Florio, G., & Rapolla, A. (2005). Multiscale derivative analysis of the gravity and magnetic fields of Southern Apennines (Italy). CROP Project. In I.Finetti (Ed.), *Deep seismic exploration of the Central Mediterranean and Italy (Atlases in Geoscience)* (Vol. 1, pp. 281–318). Elsevier Science.
- Fedi, M., & Florio, G. (2001). Detection of potential fields source boundaries by enhanced horizontal derivative method. *Geophysical Prospecting*, 49(1), 40–58. <https://doi.org/10.1046/j.1365-2478.2001.00235.x>
- Fedi, M., & Rapolla, A. (1993). *I metodi gravimetrico e magnetico nella geofisica della Terra solida*.
- Finetti, I. (1983). Struttura ed evoluzione della microplacca adriatica. *Bollettino di Geofisica Teorica ed Applicata*, II(2), 115–123.
- FitzGerald, D., & Milligan, P. (2013). Defining a deep fault network for Australia, using 3D'worming'. *ASEG Extended Abstracts*, 2013(1), 1–4. <https://doi.org/10.1071/ASEG2013ab135>
- Fu, L.-L., & Cazenave, A. (2000). *Satellite altimetry and Earth sciences: A handbook of techniques and applications*. Elsevier.
- Fukushima, T. (2019). *Fast computation of prismatic gravitational field*.
- Gantar, C. (1983). *Rilievo gravimetrico offshore mgb002: Sullo zoccolo continentale nel mare Adriatico, per l'Agip Mineraria*. Osservatorio Geofisico Sperimentale (OGS). Rel. 5/83 - MNS/ N. 82595.
- Green, C., Fletcher, K., Cheyney, S., Dawson, G., & Campbell, S. (2019). Satellite gravity – Enhancements from new satellites and new altimeter technology. *Geophysical Prospecting*, 67(6), 1611–1619. <https://doi.org/10.1111/1365-2478.12697>
- Hildebrand, J. A., Stevenson, J. M., Hammer, P. T. C., Zumbrage, M. A., Parker, R. L., Fox, C. G., & Meis, P. J. (1990). A seafloor and sea surface gravity survey of Axial Volcano. *Journal of Geophysical Research*, 95(B8), 12751–12763. <https://doi.org/10.1029/JB095iB08p12751>
- Hinze, W. J., Aiken, C., Brozena, J., Coakley, B., Dater, D., Flanagan, G., et al. (2005). New standards for reducing gravity data: The North American gravity database. *Geophysics*, 70(4), J25–J32. <https://doi.org/10.1190/1.1988183>
- Hofmann-Wellenhof, B., & Moritz, H. (2006). *Physical geodesy*. Springer Science & Business Media.
- Luyendyk, B. P. (1984). On-bottom gravity profile across the East Pacific Rise crest at 21 north. *Geophysics*, 49(12), 2166–2177. <https://doi.org/10.1190/1.1441632>
- Mastronuzzi, G., Palmentola, G., & Sansò, P. (2002). Lineamenti e dinamica della costa pugliese. *Studi Costieri*, 5, 9–22.
- Miller, H. G., & Singh, V. (1994). Potential field tilt—A new concept for location of potential field sources. *Journal of Applied Geophysics*, 32(2–3), 213–217. [https://doi.org/10.1016/0926-9851\(94\)90022-1](https://doi.org/10.1016/0926-9851(94)90022-1)
- Morelli, C. (1966). The geophysical situation in Italian waters. *International Hydrographic Review*.
- Morelli, D. (2002). Evoluzione tettonico-stratigrafica del Margine Adriatico compreso tra il Promontorio garganico e Brindisi. *Mémoires de la Société Géologique Itali*, 57, 343–353.
- Nagy, D., Papp, G., & Benedek, J. (2000). The gravitational potential and its derivatives for the prism. *Journal of Geodesy*, 74(7–8), 552–560. <https://doi.org/10.1007/s001900000116>
- Nagy, D., Papp, G., & Benedek, J. (2002). Corrections to “The gravitational potential and its derivatives for the prism”. *Journal of Geodesy*, 76(8), 475. <https://doi.org/10.1007/s00190-002-0264-7>
- Nowell, D. A. (1999). Gravity terrain corrections—An overview. *Journal of Applied Geophysics*, 42(2), 117–134. [https://doi.org/10.1016/S0926-9851\(99\)00028-2](https://doi.org/10.1016/S0926-9851(99)00028-2)
- Parker, R. L. (1973). The rapid calculation of potential anomalies. *Geophysical Journal International*, 31(4), 447–455. <https://doi.org/10.1111/j.1365-246X.1973.tb06513.x>

- Pavlis, N. K., Holmes, S. A., Kenyon, S. C., & Factor, J. K. (2012). The development and evaluation of the Earth Gravitational Model 2008 (EGM2008). *Journal of Geophysical Research*, 117(B4). <https://doi.org/10.1029/2011JB008916>
- Rapolla, A. (1986). Crustal structure of Central and Southern Italy from gravity and magnetic data. *Giornale di Geologia*, 48(1–2), 129–143.
- Ridente, D., Fracassi, U., Di Bucci, D., Trincardi, F., & Valensise, G. (2008). Middle Pleistocene to Holocene activity of the Gondola fault zone (southern Adriatic foreland): Deformation of a regional shear zone and seismotectonic implications. *Tectonophysics*, 453(1–4), 110–121. <https://doi.org/10.1016/j.tecto.2007.05.009>
- Ridente, D., & Trincardi, F. (2006). Active foreland deformation evidenced by shallow folds and faults affecting late Quaternary shelf-slope deposits (Adriatic Sea, Italy). *Basin Research*, 18(2), 171–188. <https://doi.org/10.1111/j.1365-2117.2006.00289.x>
- Sandwell, D. T. (1992). Antarctic marine gravity field from high-density satellite altimetry. *Geophysical Journal International*, 109(2), 437–448. <https://doi.org/10.1111/j.1365-246X.1992.tb00106.x>
- Sandwell, D. T., Garcia, E., Soofi, K., Wessel, P., Chandler, M., & Smith, W. H. F. (2013). Toward 1-mGal accuracy in global marine gravity from CryoSat-2, Envisat and Jason-1. *The Leading Edge*, 32(8), 892–899. <https://doi.org/10.1190/tle32080892.1>
- Sandwell, D. T., Müller, R. D., Smith, W. H. F., Garcia, E., & Francis, R. (2014). New global marine gravity model from CryoSat-2 and Jason-1 reveals buried tectonic structure. *Science*, 346(6205), 65–67. <https://doi.org/10.1126/science.1258213>
- Sandwell, D. T., & Smith, W. H. (2009). Global marine gravity form retracked Geosat and ERS-1 altimetry: Ridge segmentation versus spreading rate. *Journal of Geophysical Research*, 10. <https://doi.org/10.1029/2008JB006008>
- Stacey, F. D., & Tuck, G. J. (1981). Geophysical evidence for non-Newtonian gravity. *Nature*, 292(5820), 230–232. <https://doi.org/10.1038/292230a0>
- Talwani, M., Early, W. P., & Hayes, D. E. (1966). Continuous analog computation and recording of cross-coupling and off-leveling errors. *Journal of Geophysical Research*, 71(8), 2079–2090. <https://doi.org/10.1029/JZ071i008p02079>
- Tramontana, M., Morelli, D., & Colandoni, P. (1995). Tettonica plio-quaternaria del sistema sud-garganico (settore orientale) nel quadro evolutivo dell'Adriatico centro-meridionale. *Studi geologici camerti, n. speciale, 1995* (pp. 467–473).
- Uieda, L., Soler, S. R., Pesce, A., Oliveira, V. C., Jr., & Shea, N. (2020). *Harmonica: Forward modeling, inversion, and processing gravity and magnetic data (version v0.1.0)*. <https://doi.org/10.5281/zenodo.3628742>
- Volpi, V., Forlin, E., Baroni, A., Estublier, A., Donda, F., Civile, D., et al. (2015). Evaluation and characterization of a potential CO₂ storage site in the south Adriatic offshore. *Oil & Gas Science and Technology—Revue d'IFP Energies Nouvelles*, 70(4), 695–712. <https://doi.org/10.2516/ogst/2015011>
- Wessel, P., Luis, J. F., Uieda, L., Scharroo, R., Wobbe, F., Smith, W. H., & Tian, D. (2019). The generic mapping tools version 6. *Geochemistry, Geophysics, Geosystems*, 20(11), 5556–5564. <https://doi.org/10.1029/2019GC008515>
- Wijns, C., Perez, C., & Kowalczyk, P. (2005). Theta map: Edge detection in magnetic data. *Geophysics*, 70(4), L39–L43. <https://doi.org/10.1190/1.1988184>